JMEPEG
https://doi.org/10.1007/s11665-023-08624-8

1059-9495/$19.00

ORIGINAL RESEARCH ARTICLE

Analysis of the Anti-corrosion Performance of Dodecyl Benzene Sulfonic Acid Sodium Salt on Various Heat-Treated Dual-Phase EN8 Steel in an Acidic Environment

Deepa Prabhu, Jilna Jomy, and P.R. Prabhu

Submitted: 5 April 2023 / Revised: 5 July 2023 / Accepted: 4 August 2023

This work focuses on the investigation of the corrosion inhibition of heat-treated EN8 steel in the presence of sodium salt of dodecyl benzene sulfonic acid in 0.5 M H_2SO_4 using the Gravimetric and Electrochemical methods. Austenitizing is performed at 700, 750, 790, and 900 °C for 2 h followed by quenching in water. When the heat-treated metal is exposed to 0.5 M H_2SO_4 at the temperature of 30, 40, 50, and 60 °C in the presence of dodecyl benzene sulfonic acid sodium salt inhibitor, the corrosion inhibition increased with different heat treatment conditions depending on the phase change. This work investigates the activation and adsorption isotherm parameters. The adsorption isotherms were used to estimate Gibb's free energy change. The inhibition efficiency increased with inhibitor concentration and decreased with temperatures. Out of all the isotherms examined, the Langmuir adsorption isotherm produced the best-fit results, according to the adsorption study. Corrosion and inhibition on the metal's surface were confirmed by surface characterization.

Keywords EN8 steel, electrochemical studies, gravimetric method, heat treatment, H_2SO_4, SEM, XRD

1. Introduction

In petroleum industries, the use of alloy steel is commonly used for the fabrication of materials such as tanks, pipelines, and heat exchangers (Ref 1, 2). These pipelines are commonly used for transportation, mining, and storage of crude oil. Since the oil and gas industry contributes a major share in economic development, scientists are interested in understanding the damage caused by corrosion in these pipelines due to corrosion, during acid well cleaning (Ref 3). Another important impact of the corrosion study is that it helps to avoid potential disasters arising due to leakage, which can negatively impact human life and may lead to environmental pollution (Ref 4).

Acids are utilized in these pipelines for scale removal treatment such as pickling and removal of drilling mud damage. It is also used for the well-acidizing procedure, which involves the injection of acids into steel tubes (Ref 4). During these procedures, steel comes in contact with acids that causes corrosion. One of the commonly used steel alloys in the petroleum industry is medium carbon steel. This is due to its easy availability, high strength, and low cost. A type of medium carbon steel is EN8 or AISI 1040 steel. EN8 steel is characterized by its good tensile strength and high machinability. This steel can be heat treated to achieve uniform homogenous structures which improve the machinability and corrosion resistance of the metals.

Heat treatment is a procedure in which a metal is heated to an austenite crystal phase and is cooled by furnace cooling or rapid quenching in water/oil. This leads to a change in the microstructures of the crystal lattice (Ref 5, 6). There are different types of heat treatment procedures such as annealing, normalizing, and quenching (Ref 7). Normalizing involves heating the metal to a temperature higher than its annealing temperature followed by air cooling. This leads to a reduction in the stress in the crystal lattice and more stability for the structure. Quenching involves rapid cooling of the metal in water or oil after heating. This makes the metal hard but brittle. The influence of various heat treatment procedures on the mechanical and corrosion resistance of the metals attained considerable attention from researchers (Ref 1, 8–10). Oguzhan Keleştemur et al. investigated the effect of various heat treatments on the corrosion resistance of dual-phase reinforcing steel. It was found that the corrosion rate decreases with an increase in the martensite phase of the metal (Ref 11). Omid Abedini et al. studied the influence of inter-critical heat treatment temperature on the corrosion resistance and mechanical properties of dual-phase steel. It was found that the corrosion resistance of dual-phase steel was higher than the as-received metal specimen (Ref 12). Wilson Handoko et al. analyzed the effect of austenitization temperature on the corrosion resistance of high-carbon steel. Results indicated a

Deepa Prabhu, Department of Chemistry, Manipal Institute of Technology Bengaluru, Manipal Academy of Higher Education, Manipal, Karnataka 576104, India; **Jilna Jomy**, Department of Chemistry, Manipal Institute of Technology, Manipal Academy of Higher Education, Manipal, Karnataka 576104, India; and **P.R. Prabhu**, Department of Mechatronics, Manipal Institute of Technology, Manipal Academy of Higher Education, Manipal, Karnataka 576104, India. Contact e-mail: raghu.prabhu@manipal.edu.

Published online: 23 August 2023

reduction in the corrosion resistance with an increase in the austenitizing temperature due to the increase in the number of carbide precipitates (Ref 9).

Another major method employed for corrosion protection is the use of corrosion inhibitors (Ref 13-17). One of the most commonly used corrosion inhibitors is surfactants. Surfactants are amphiphilic molecules constituting a hydrophilic part along with a hydrophobic part. The hydrophilic part consists of positively or negatively charged ions and the hydrophobic part consists of hydrocarbon chains. Due to this behavior, it can be solubilized in both oil and water, thus these molecules can have a high influence on the properties of surfaces and interfaces. This phenomenon of surfactants gained interest in researchers in the potential use of surfactants as corrosion inhibitors (Ref 18). Shalabi et al. have studied a new pyridinium bromocationic surfactant (DHPB) as a corrosion inhibitor for carbon steel and found that the inhibition efficiency increased with an increase in the concentration of DHPB and temperature (Ref 19). Mostafa H. Sliem et al. investigated the corrosion inhibition efficiency of the AEO7 surfactant for carbon steel in an HCl medium. An enhancement in the corrosion resistance as well as a decrease in the surface roughness was observed when AEO7 surfactant was used (Ref 20).

This work aims to investigate the effect of the addition of Sodium dodecyl benzene sulfonic acid (SBDS) surfactant on the corrosion resistance of heat-treated dual-phase EN8 steel in 0.5 M sulfuric acid medium. The inhibition efficiency was evaluated using weight loss (WL), potentiodynamic polarization study (PDP), and electrochemical impedance study (EIS). The kinetic, thermodynamic factors, and adsorption isotherms were considered to validate the mechanism of inhibition. Furthermore, the adsorption of inhibitor on the surface was confirmed using SEM analysis.

2. Experimental Techniques

2.1 Material and Heat Treatment Process

The EN8 steel specimen composed of Fe (98.7%), C (0.247%), Si (0.199%), Mn (0.54%), P (0.027), S (0.037%), Cr (0.095%), Ni (0.044%), Cu (0.059), Mo (0.027%). The heat-treated test samples were made from cylindrical rods with a diameter of 19 mm and a height of 8 mm. The specimen was polished from course to fine emery papers of 80-800 and ultra-fine polishing is done using disk polisher & polishing cloth using diamond paste (3-0.25 microns) (Ref 21).

2.2 Heat Treatment

Initially, the samples were heated in an electric muffle furnace [Make: ROTEK, Model: RMF-4] at the predetermined austenitization temperature (900 °C). The process PQ represents the austenitization process. The samples were kept at the austenitization temperature for a fixed duration of 2 h. After isothermal holding for 2 h, specimens are quickly taken out from the furnace for air cooling to get the room temperature structure (Fig. 1a). Austenitizing is carried out at 700, 750, 790, and 900 °C for 2 h followed by then quenching in water to form dual-phase structure (Fig. 1b).

2.3 Corrosive Medium and Inhibitor

The medium used for the investigation is standard sulfuric acid. Analytical grade sulfuric acid procured and used. A solution of 0.5 M concentration was prepared by the appropriate dilution of the stock solution. The experiments were carried out at varying temperatures of 30, 40, 50, and 60 °C (Ref 21, 22). Commercially available Dodecyl benzene sulfonic acid sodium salt (SBDS) (Ref 23) surfactant was procured for the present work from Loba Chemie Pvt. Ltd (CAS-No.: 25155-30-0 MSDS). The corrosion studies were carried out in 0.0025, 0.005, 0.0075, and 0.01 M concentrations of SBDS.

2.4 Gravimetric Method

The method is carried out as per a standard method (e.g., ASTM G1-90, 1996) (Ref 24). Although it is possible to run a large number of samples simultaneously, weight loss methods typically operate at a slower pace than other methods. The rate of corrosion was calculated from the expression $CR = \frac{KW}{ATD}$, where, W = difference between the initial and final weight of the sample (gms), $K = 3.45 \times 10^6$, A = area (cm^2), T = im-

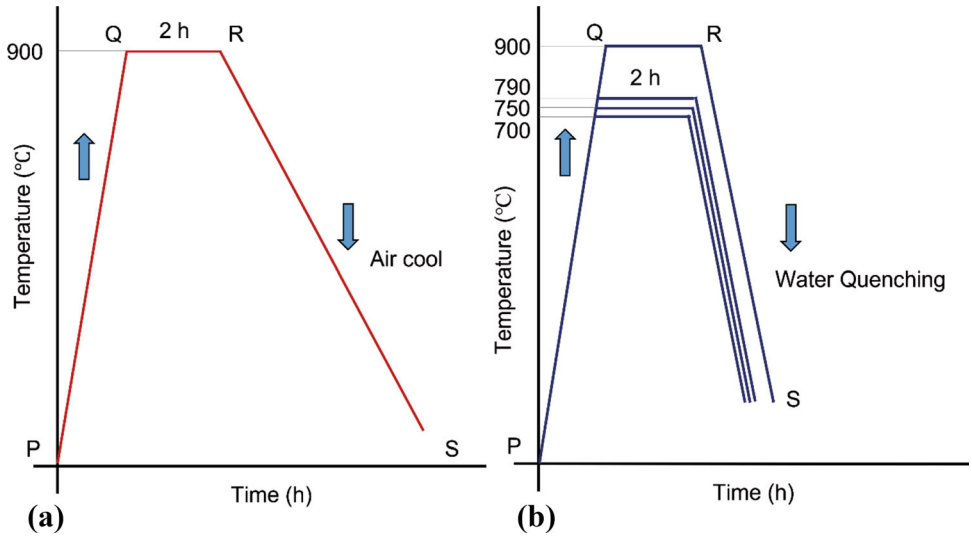

Fig. 1 (a) Normalizing heat treatment cycle and (b) Heat treatment procedure for obtaining dual-phase structure

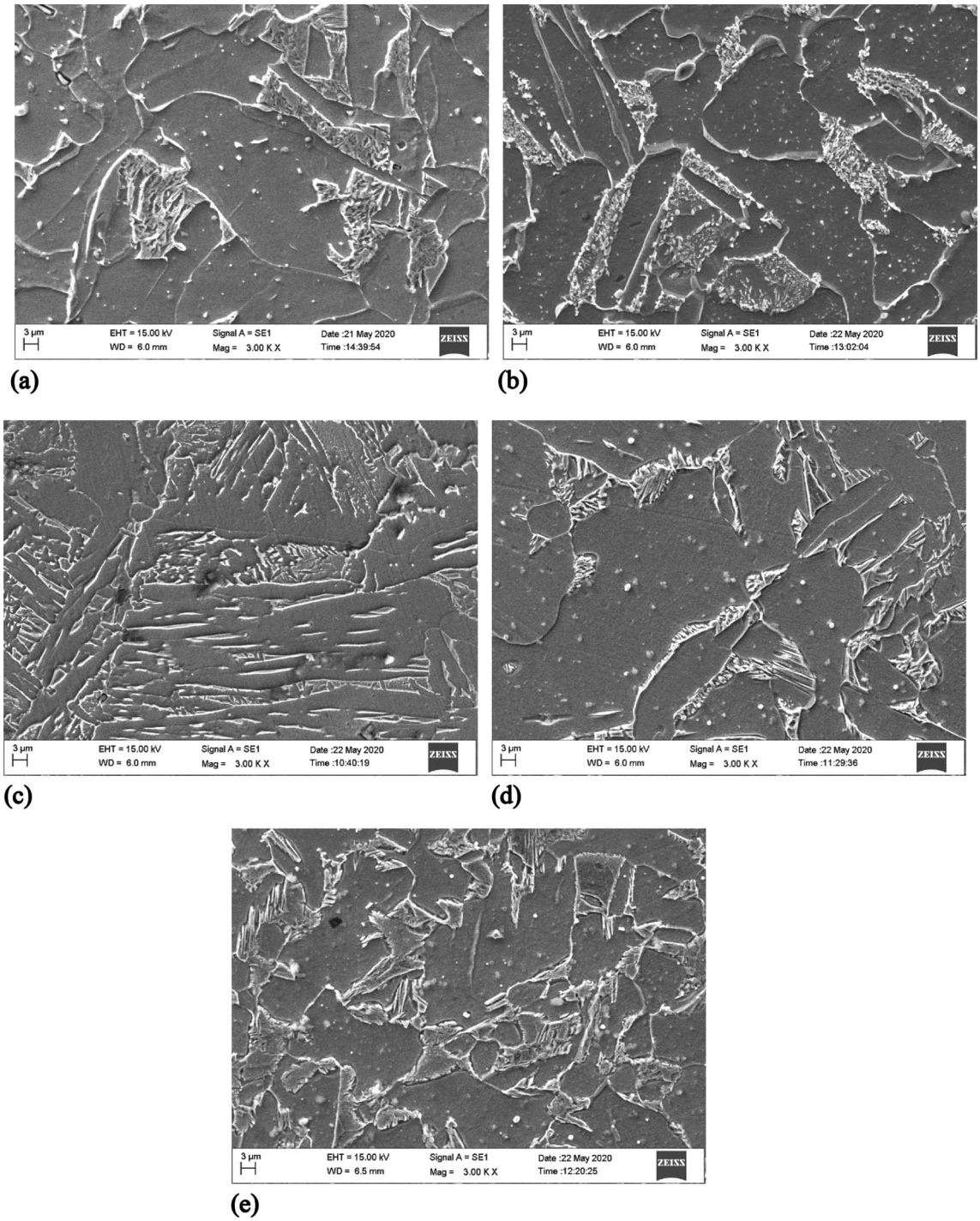

Fig. 2 SEM images of heat treated EN 8 steel (a) Normalized (b) Quenched at 700 °C (c) Quenched at 750 °C (d) Quenched at 790 °C (e) Quenched at 900 °C

mersion time (hours), D = density (g/cm^3) (Ref 7). The inhibition efficiency (IE) was obtained by $\mathrm{IE}(\%) = \frac{(W1-W2)}{W1} \times 100$, where, $W1$ = weight of metal without inhibitor (grams), $W2$ = weight of metal with inhibitor (grams). ($W1$ and $W2$ are noted based on the difference between the initial and final weight of the samples before and after exposure) (Ref 25). The Kinetic parameters like activation energy (E_a) were calculated from the CRs at various temperatures by $\ln(\mathrm{CR}) = B - E_a RT$, where R = 8.314 J mol^{-1} K^{-1}, T = absolute temperature (K), and B = a constant, which varies for different metals. The activation enthalpy ($\Delta H^{\#}$), and activation entropy ($\Delta S^{\#}$) were calculated using $\mathrm{CR} = \frac{RT}{\mathrm{Nh}} \exp\left(\frac{\Delta S^{\#}}{R}\right) \exp\left(\frac{\Delta H^{\#}}{RT}\right)$, where h = Plank's constant (6.626 × 10^{-34} J.s), N = Avogadro's number (6.022 × 10^{23} mol^{-1}), and T = absolute temperature (K) (Ref 26). The adsorption isotherm and thermodynamic parameters

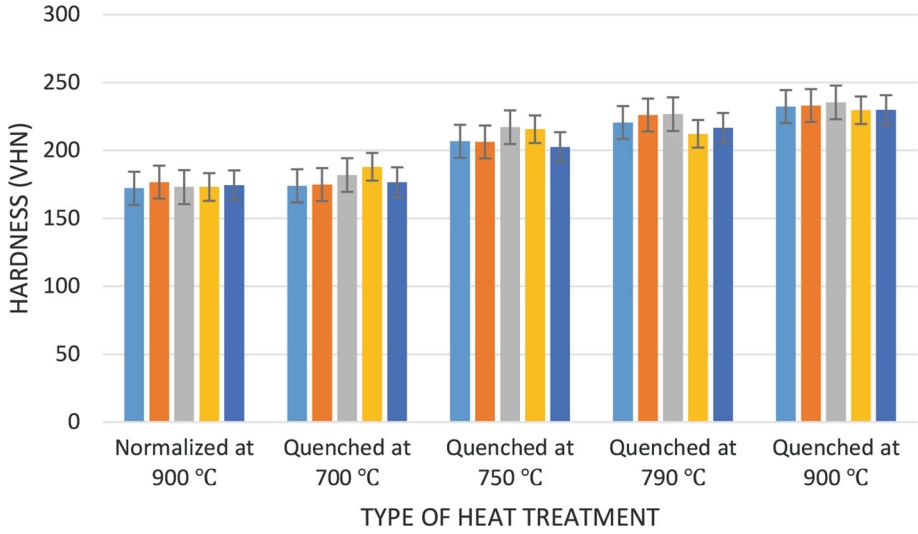

Fig. 3 Hardness of heat-treated materials of EN8 steel

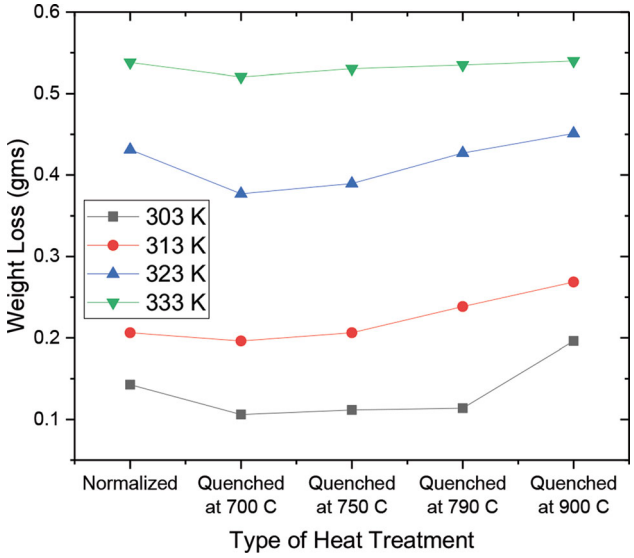

Fig. 4 Weight loss plots of heat-treated materials in 0.5 M H_2SO_4 at different temperatures

where obtained by the interaction of SBDS molecules with the metal surfaces is described by adsorption isotherm. The best possible adsorption isotherm is chosen based on the correlation coefficient (R^2) and best fits. The adsorption equilibrium constant (K) served as the foundation for the calculation of the standard free adsorption energy ($\Delta G°_{ads}$) (Ref 27).

2.5 EIS and PDP Method

The electrochemical setup was used to measure electrochemical impedance study (EIS) and potentiodynamic polarization study (PDP) measurements (Ref 28). To measure EIS and PDP, a mouldable EN8 steel sample with an exposed surface area of 0.7 cm^2 served as the working electrode. As the counter electrode and the reference electrode, respectively, the platinum electrode and the calomel electrode were utilized. The potentiostat CH600E was connected to all three electrodes, which were submerged in the corrosive medium (0.5 M H_2SO_4). Under aerated, unstirred conditions, the electrochemical measurements were carried out at a temperature of 30 °C. A sinusoidal AC voltage amplitude of 10 mV and a frequency range of 100 to 10 Hz have been chosen for EIS measurements. The working electrode was polarized for the PDP studies at the open circuit potential from − 250 mV (cathodically) to + 250 mV (anodically) with a scan rate of 1.0 mVs^{-1} (Ref 29, 30).

2.6 Scanning Electron Microscopy (SEM) and x-ray Diffraction (XRD) Analysis

SEM was used to determine the heat-treated (normalized, quenched at 700, 750, 790, and 900 °C) EN8 steel's surface morphology. The SEM images were obtained with an EVO MA18 at a magnification of 3000× and 500×. Minifex 600 model instruments were used to take XRD images of different heat-treated EN8 steel samples.

3. Result and Discussion

3.1 Heat Treatment

The microstructure exhibit fine and lamellar pearlite and proeutectoid ferrite in Fig. 2(a) microstructure of EN 8 steel in the normalized condition. Steel's mechanical properties are enhanced by fine pearlite. Figure 2(b), (c), (d), (e) shows the ferrite and martensite-rich microstructure. The austenite transforms into martensite while the proeutectoid ferrite remains unchanged when the steel is quenched in liquid at room temperature and held at inter-critical temperatures. The carbon atoms do not get enough time to diffuse out of austenite during the cooling process, resulting in a distorted martensite structure.

The MATZUAWA Micro Vickers hardness tester was used to measure the samples' surface hardness. The microhardness variations between two successive indentations are evaluated using the Vickers indentor, which was loaded with 4.905 N for a loading period of ten seconds. The hardness of the heat-

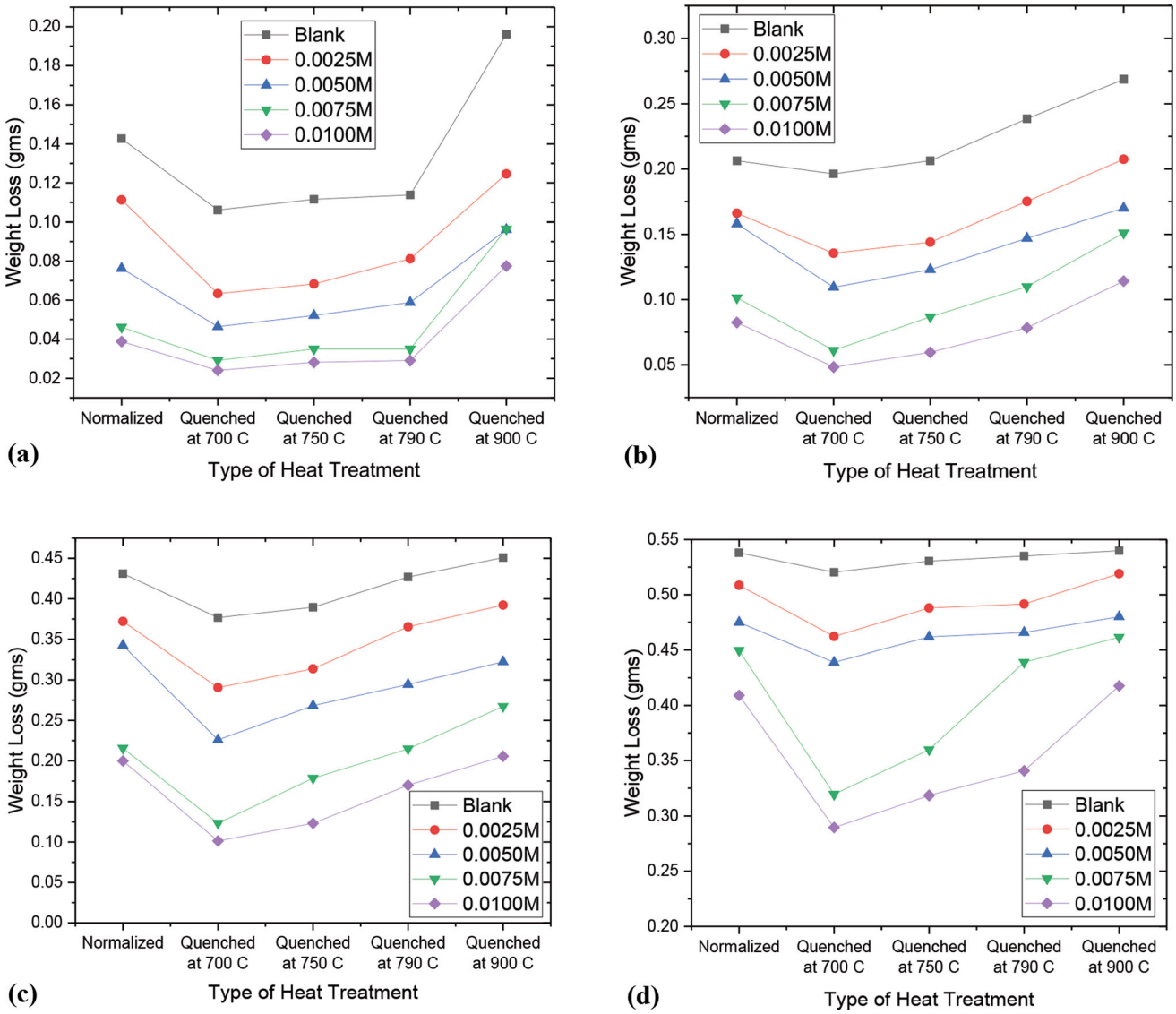

Fig. 5 Weight loss plots in 0.5 M H_2SO_4 containing different concentrations of SBDS at (a) 303 K (b) 313 K (c) 323 K (d) 333 K for the corrosion of different heat-treated materials

treated material increased with an increase in the austenitization temperatures from 700, to 900 °C as given in Fig. 3. The variations observed in the microhardness within the same samples prove the presence of inhomogeneity in the crystal sizes and phases (Ref 31). The minimum microhardness value was observed for normalized EN 8 steel and the improvement of microhardness value was observed with an increase in heat treatment temperature. This change in the hardness value is due to the difference in the rate of cooling during solidification and the amount of martensite phase present (Ref 32). With an increase in the amount of martensite phase, the carbon content of the metal increases. This results in an increase in the microhardness with heat treatment temperature.

3.2 Corrosion Rate (CR) and Inhibition Efficiency (IE) by Weight Loss Method

The corrosion behavior of various heat-treated materials at different temperatures are given in Fig. 4. IE, WL, and CR for 0.0025, 0.005, 0.0075, and 0.01 M SBDS concentrations at 303, 313, 323, and 333 K are presented in Fig. 5, for different heat treated EN8 steel. From Fig. 5, it is seen that the IE increased with inhibitor concentration.

Figure 5 depicts the weight loss data plots of heat-treated EN8 steel in 0.5 M H_2SO_4 at various temperatures. The weight loss of all specimens was found to increase with the temperature exposed, indicating an increase in corrosion in relation to the environment's temperature. For all the heat-treated materials, a higher rate of corrosion is indicated by the increase in weight loss with raise in temperature.

The corrosion inhibition studies reveal that higher the concentration of SBDS, the lower the weight loss we measured, i.e., the higher the corrosion inhibition efficiency (IE%) up to an optimal amount of SBDS addition. This observation is due to the ability of SBDS to adsorbed on the surface of the positively charged metal surface because of the existence of oxygen atoms present in the head part of SBDS molecules

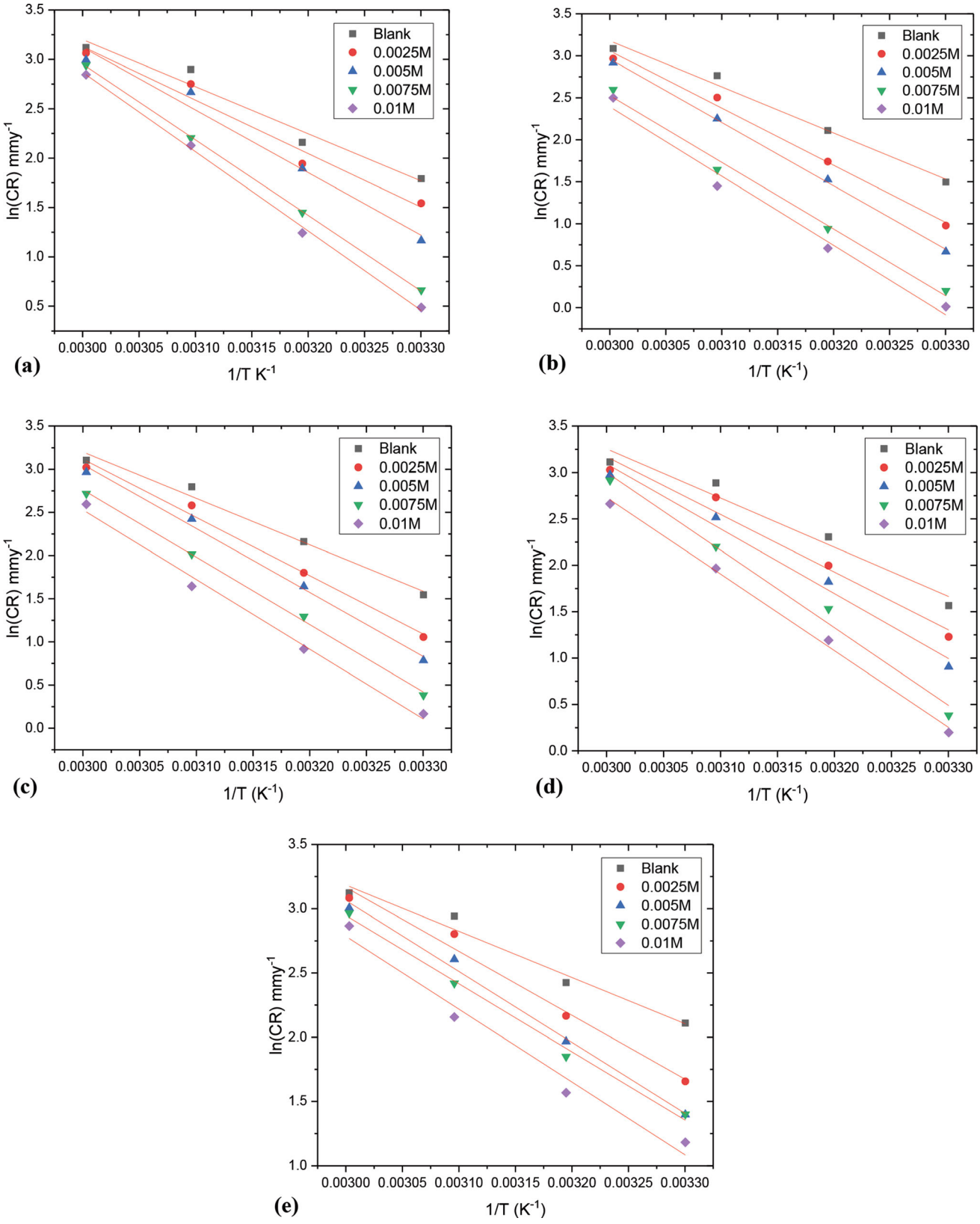

Fig. 6 Arrhenius plots for (a) Normalized (b) Quenched at 700 °C (c) Quenched at 750 °C (d) Quenched at 790 °C (e) Quenched at 900 °C heat treated EN8 in 0.5 M H_2SO_4 with SBDS inhibitor

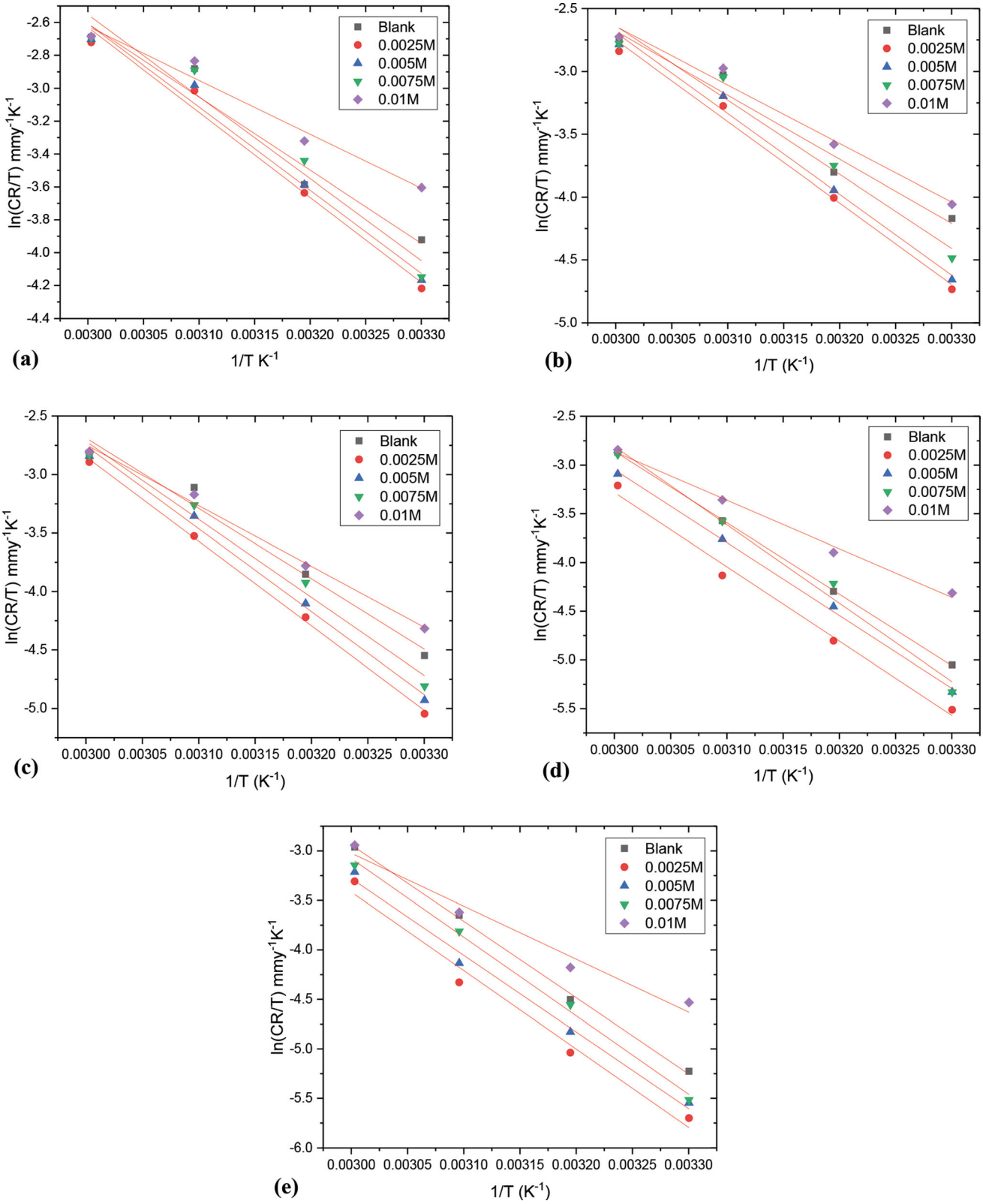

Fig. 7 Plots of ln(CR/T) vs. 1/T for (a) Normalized (b) Quenched at 700 °C (c) Quenched at 750 °C (d) Quenched at 790 °C (e) Quenched at 900 °C heat treated EN8 in 0.5 M H_2SO_4 with SBDS inhibitor

Table 1 Activation factors for heat-treated EN 8 containing SBDS in 0.5 M H_2SO_4

Material	[SBDS], M	E_a, kJ mol^{-1}	$\Delta H^{\#}$, kJ mol^{-1}	$\Delta S^{\#}$, J mol^{-1} K^{-1}
Normalized	0.0	39.63	36.99	− 108.27
	0.0025	45.02	42.38	− 92.70
	0.005	52.69	50.06	− 69.74
	0.0075	63.64	61.01	− 38.30
	0.01	66.75	64.12	− 29.67
Quenched at 700 °C	0.0	45.61	42.97	− 90.49
	0.0025	56.55	53.92	− 58.68
	0.005	62.70	60.06	− 41.06
	0.0075	66.04	63.41	− 34.64
	0.01	68.55	65.92	− 28.22
Quenched at 750 °C	0.0	44.69	42.06	− 93.07
	0.0025	51.70	49.06	− 72.30
	0.005	58.12	55.48	− 53.70
	0.0075	69.53	66.89	− 20.22
	0.01	68.62	65.98	− 25.20
Quenched at 790 °C	0.0	44.08	41.44	− 94.47
	0.0025	51.70	49.06	− 72.30
	0.005	58.12	55.48	− 53.70
	0.0075	69.53	66.89	− 20.22
	0.01	68.62	65.98	− 25.20
Quenched at 900 °C	0.0	29.88	27.24	− 137.65
	0.0025	41.35	38.71	− 103.41
	0.005	45.89	43.26	− 90.61
	0.0075	44.09	41.45	− 97.02
	0.01	47.13	44.49	− 89.23

which supports the 3d orbitals of Fe atom to interact with the lone pairs of electrons from the oxygen atoms (Ref 20, 33). As a result, the corrosion IE% goes up. As a result, when SBDS is present, the corrosion rate is a sign of how many free corrosion sites remain after the adsorbed inhibitor molecule effectively blocks the other sites (Ref 20, 34).

3.3 Kinetic Factors

Figure 6 and 7 depicts the Arrhenius plots and the EN8 steel plot of ln (CR/T) versus 1/T under various heat treatment conditions and immersion temperatures. Table 1 depicts the various activation parameters for EN 8 steel in 0.5 M H_2SO_4. The activation energy (E_a) is found to be greater than 20 kJ mol^{-1}, indicating that surface reactions control the process of oxidation due to activation polarization (Ref 35). The enthalpy of activation ($\Delta H^{\#}$) is in line with the energy of activation (E_a). The EN8 steel specimens' activation entropy ($\Delta S^{\#}$) is large and negative, indicating the formation of activation complex, i.e., disassociation (Ref 29). As the austenitization temperature rises, the kinetic energy of the surface molecules increases, leading to an increase in disorder, and as a result, the $\Delta S^{\#}$ value becomes more negative.

3.4 Adsorption Isotherm and Thermodynamic Parameters

At a given temperature, the adsorption amount of SBDS in the solid phase and the SBDS concentrations in the liquid phase are referred to as adsorption isotherms (Ref 36). By using adsorption isotherms, we can obtain the Gibb's free energy information by $\Delta G^{\circ}_{ads} = -RT\ln(C_{solvent}K)$, where R = 8.314 J mol^{-1} K^{-1}, T = Temperature in Kelvin, $C_{solvent}$ = 55.5 mol of water (Ref 37). It was found that Langmuir isotherms (Fig. 8) had the best fit among other isotherms. The thermodynamic parameters associated with the adsorption process are determined Fig. 9 and the results are presented in Table 2.

With SBDS, the ΔG°_{ads} were in the range of −18 to −25 kJ mol^{-1} (Ref 38). The ΔG°_{ads} value moved from more negative to less negative with the increase in T (Table 2), proposing the physical adsorption of SBDS on the surface of metals (Ref 39). The fact that the adsorption enthalpy (ΔH°_{ads}) was negative confirms physisorption and points to an exothermic process. The positive and large adsorption entropy (ΔS°_{ads}) indicates that the inhibitor molecules were arranged systematically on the surface (Ref 40).

3.5 Potentiodynamic Polarization

Figure 10 shows the Tafel plot obtained by corroding EN8 steel at 303 K in a 0.5 M H_2SO_4 solution under various heat treatment conditions (normalized, quenched at 700, 750, 790, and 900 °C) with varying concentrations of SBDS. The obtained i_{corr} values (Table 3) indicate active dissolution of the metal. The EN8 steel that is quenched at 700 °C has the lowest i_{corr} value, indicating that it is more resistant to corrosion. The value of i_{corr} rises with the rise in the quenching temperature, which ranges from 700 to 900 °C. This suggests that as the heat treatment temperature rises, the rate of corrosion has also raised. The i_{corr} value of the normalized EN 8 steel was found to be lesser than the quenched specimens, which indicates a greater corrosion resistance for the normalized specimen than the other.

The fact that there was no significant variation in the values of the obtained anodic and cathodic Tafel slopes (β_a) and (β_c) suggests that there was no change in the mechanism of the anodic and cathodic processes when SBDS was present (Ref

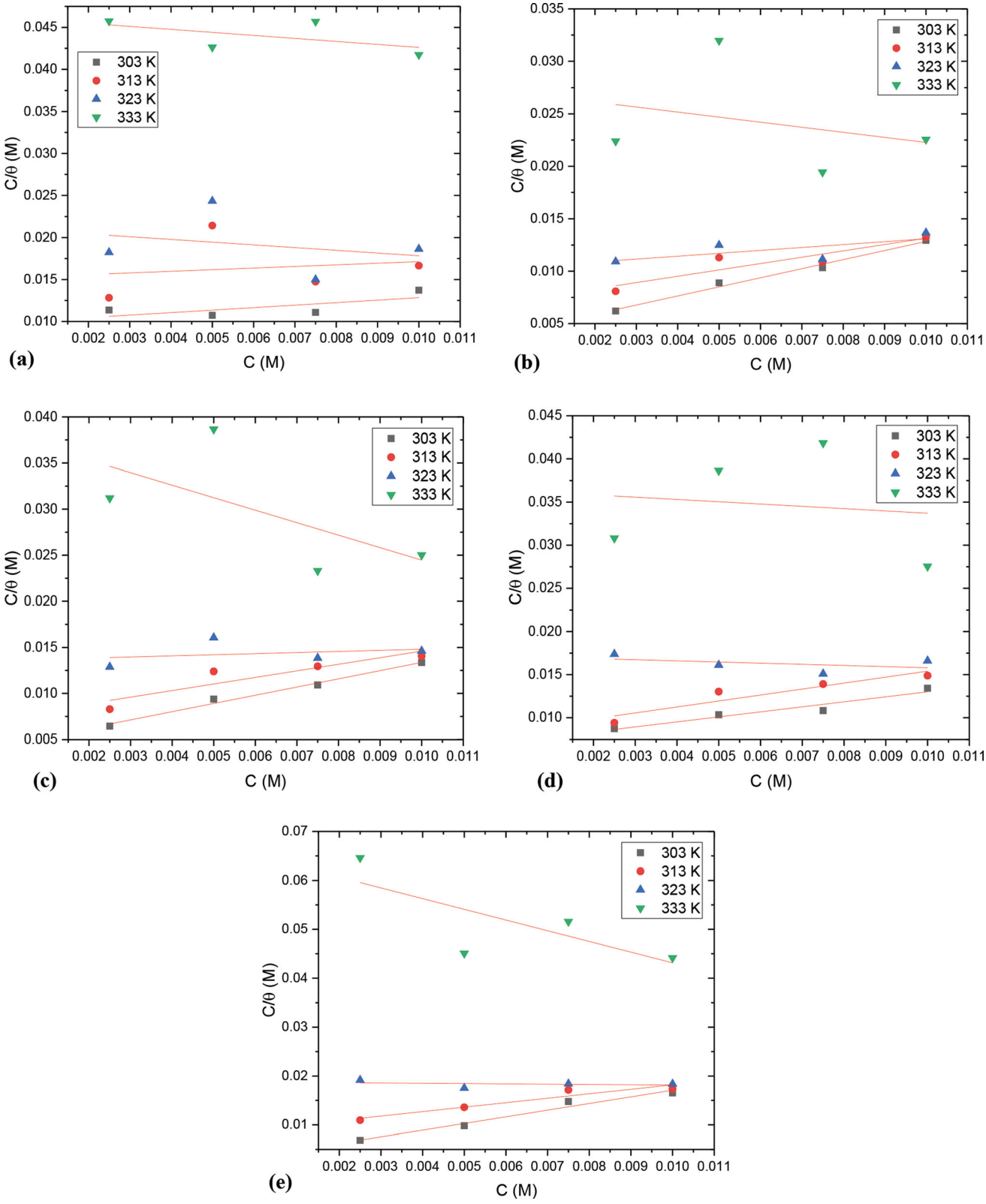

Fig. 8 (a) Langmuir adsorption isotherms for (a) Normalized (b) Quenched at 700 °C (c) Quenched at 750 °C (d) Quenched at 790 °C (e) Quenched at 900 °C heat treated EN8 in 0.5 M H_2SO_4 with SBDS inhibitor

41). Riggs says that if the corrosion potential value (E_{corr}) was less than ± 85 mV on average,(Ref 42) suggests that the inhibitor act as a mixed type of inhibitor. As the inhibitor concentration increased, the i_{corr} values decreased, indicating a decrease in corrosion activity and an increase in the IE. The highest inhibition was observed for EN 8 steel quenched at

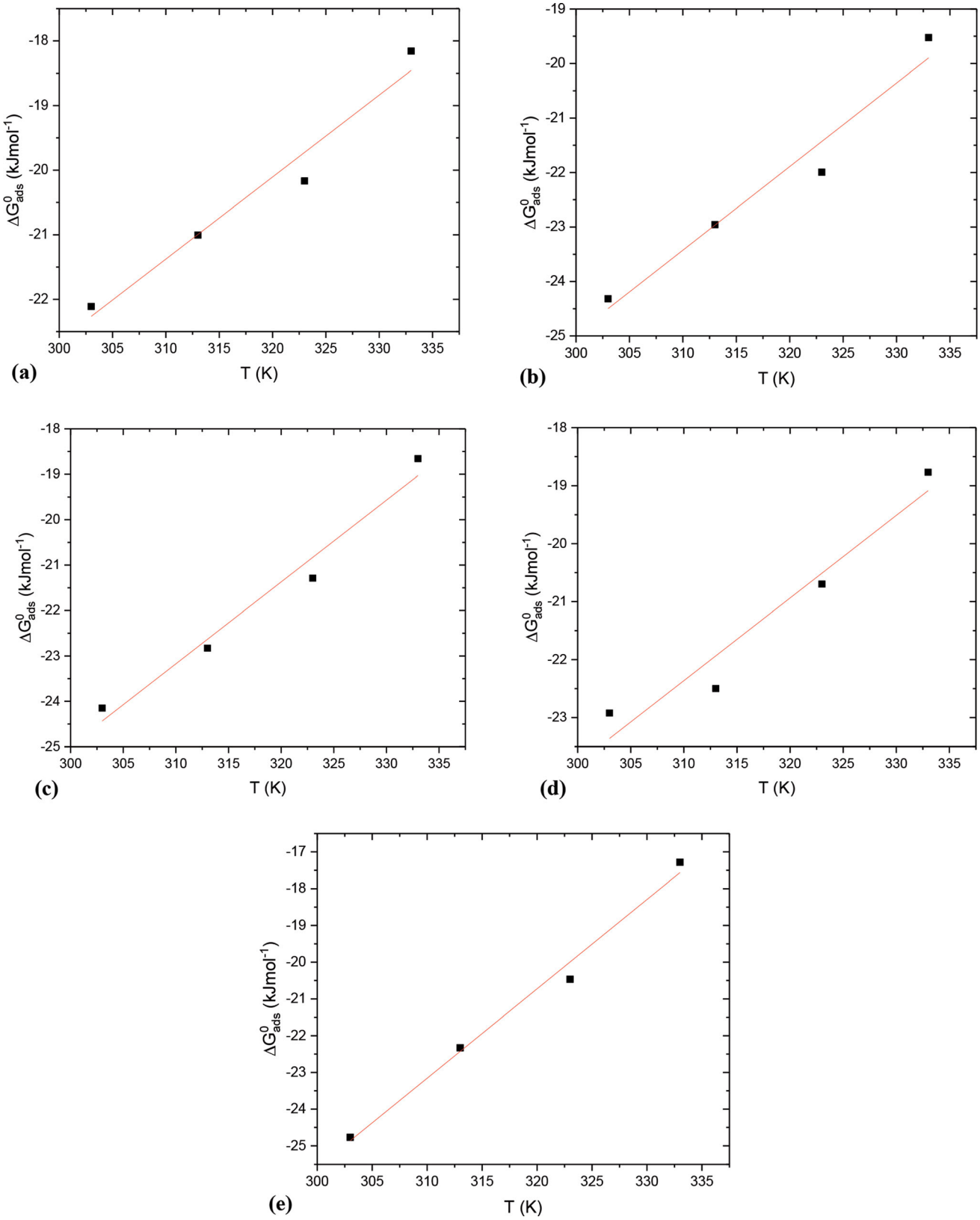

Fig. 9 Plot of ΔG°_{ads} vs. T for (a) Normalized (b) Quenched at 700 °C (c) Quenched at 750 °C (d) Quenched at 790 °C (e) Quenched at 900 °C heat treated EN8 in 0.5 M H_2SO_4 with SBDS inhibitor

Table 2 Thermodynamic factors for the adsorption of different heat-treated EN8 containing SBDS in 0.5 M H_2SO_4

Material	*T*, °C	$\Delta G°_{ads}$, kJ mol^{-1}	$\Delta H°_{ads}$, kJ mol^{-1}	$\Delta S°_{ads}$, J mol^{-1} K^{-1}	R^2
Normalized	30	− 22.11	− 60.72	126.93	0.96
	40	− 21.00			
	50	− 20.16			
	60	− 18.15			
Quenched at 700 °C	30	− 24.31	− 70.96	153.36	0.95
	40	− 22.95			
	50	− 21.99			
	60	− 19.52			
Quenched at 750 °C	30	− 24.15	− 79.04	180.21	0.97
	40	− 22.82			
	50	− 21.28			
	60	− 18.65			
Quenched at 790 °C	30	− 22.92	− 66.55	142.55	0.94
	40	− 22.49			
	50	− 20.69			
	60	− 18.77			
Quenched at 900 °C	30	− 24.76	− 98.55	243.22	0.98
	40	− 22.32			
	50	− 20.46			
	60	− 17.28			

790 °C (85.36%) and the least observed for metal quenched at 700 °C(69.57%). The other 3 materials showed moderate efficiency laying between 69 and 85% efficiency.

3.6 EIS Method

Figure 11 depicts the Nyquist plot that was obtained for the EN 8 steel in 0.5 M H_2SO_4 when it was heat treated at different conditions in the absence and presence of an SBDS inhibitor. Due to the frequency dispersion effect, the Nyquist diagram depicts semicircles with a depressed capacitive loop at high frequency (HF) under various heat treatment conditions (Ref 43-45). Using ZSimpWin version 3.1 software, an equivalent circuit with R_s (Solution resistance), R_{ct} (Charge transfer resistance), and a constant phase element (CPE) was used to fit the obtained curves, as shown in Fig. 12. The values are shown in Table 4. Due to the surface's inhomogeneity, the ideal double-layer capacitance has been replaced by CPE in the circuit, resulting in the HF region's depressive capacitive loop. $C_{dl} = \frac{1}{2\pi f_{max} R_p}$, where f_{max} is the frequency maximum is used to calculate C_{dl} for this circuit. The polarization resistance (R_p) is calculated using $R_p = R_s + R_{ct}$ where R_s is solution resistance, R_{ct} is charge transfer resistance. The EN8 steel quenched at 700 °C has the highest R_p value, indicating the highest corrosion resistance when compared to other heat treatment conditions. R_p values decrease as the austenitization temperature rises from 750 to 900 °C, indicating a decrease in corrosion resistance. The corrosion behavior of EN8 steels with ferrite and martensite depends on the amount of ferrite and martensite in them. The amount of martensite rises as the austenitization temperature rises from 750 to 900 °C. As a result, the number of micro galvanic corrosion cells (lamellas) serving as active corrosion sites in the area between the ferrite and martensite phases rises (Ref 46, 47). The normalized specimen had a higher R_p value than the water-quenched specimen at 900 °C, so it was more resistant to corrosion than the water-quenched specimen. This is because normalized EN8 steel with ferrite-pearlite phase has less carbon than quenched specimen austenitized at 900 °C steel with ferrite-martensite phase (Ref 48).

3.7 SEM and EDS Analysis

Figure 13(a), (b), (c), (d), and (e) shows the SEM image of the EN8 Steel with and without SBDS in a 0.5 M H_2SO_4 medium under a variety of heat treatment conditions. As the austenitization temperature of the quenched sample rises from 700 to 900 °C, it is observed that the surface degradation brought on by corrosion increases. The dissolution of the metal and the deposits of corrosion products have resulted in a very uneven surface on the corroded specimen. Additionally, pits can be observed as a result of the separation of corrosion products from the metal's surface. The addition of 0.01 M of SBDS to 0.5 M H_2SO_4 showed a variation on the surface of metal, as shown in Fig. 13(a1), (b1), (c1), (d1), and (e1). Most of the holes are covered by SBDS creating an protective layer between the metal and the medium, thereby reducing corrosion.

The various elements that were present on the surface of EN 8 steel quenched at 790 °C were identified through EDS analysis. Figure 14 illustrates, respectively, the EDS spectra acquired on the EN 8 steel quenched at 790 °C in 0.5 M H_2SO_4. Figure 15 represents the EDS profile of EN 8 steel quenched at 790 °C in 0.5 M H_2SO_4 in presence of 0.01 M SBDS. The surface of the metal after corrosion in H_2SO_4 will have iron oxide and sulfur in a large amount due to the corrosion process. This is proven by the appearance of the oxygen and sulfur peaks in the EDS spectrum obtained for corroded metal surfaces. EDS spectra in the presence of 0.01 M SBDS showed the increased amount of carbon, the presence of

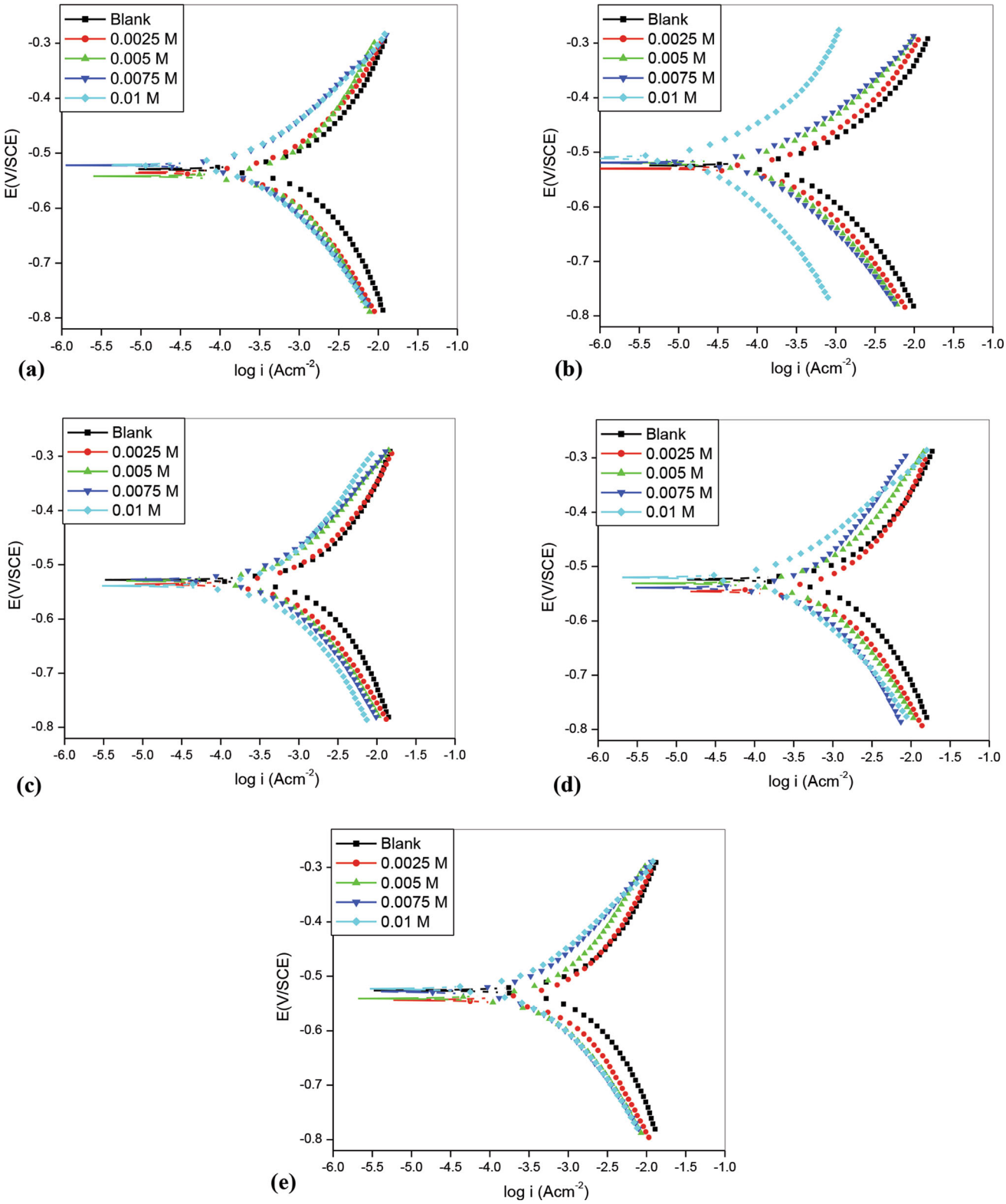

Fig. 10 PDP plots in 0.5 M H_2SO_4 containing different concentrations of SBDS at 303 K for the corrosion of (a) Normalized (b) Quenched at 700 °C (c) Quenched at 750 °C (d) Quenched at 790 °C (e) Quenched at 900 °C heat-treated phase of EN8 steel

Table 3 Results of PDP measurements for the inhibition of heat-treated EN8 steel in 0.5 M H_2SO_4 containing SBDS at 303 K

Type of heat treatment	[Surfactant], M	E_{corr}, mV versus SCE	i_{corr}, mA cm^{-2}	$-\beta_c$, m V dec^{-1}	β_a, m V dec^{-1}	*IE*, %
Normalized	0.0000	− 528	1.446	576	594	–
	0.0025	− 536	0.628	631	724	56.56
	0.0050	− 542	0.512	595	625	64.59
	0.0075	− 524	0.242	735	804	83.26
	0.0100	− 522	0.209	760	865	85.54
Quenched at 700 °C	0.0000	− 529	0.404	604	627	–
	0.0025	− 530	0.244	734	888	39.60
	0.0050	− 520	0.137	818	931	66.08
	0.0075	− 519	0.102	843	976	74.75
	0.0100	− 510	0.023	768	950	94.30
Quenched at 750 °C	0.0000	− 524	1.218	609	671	–
	0.0025	− 536	0.861	631	676	29.31
	0.0050	− 530	0.531	674	699	56.40
	0.0075	− 539	0.449	655	646	63.13
	0.0100	− 527	0.400	710	762	67.15
Quenched at 790 °C	0.0000	− 529	1.295	577	600	–
	0.0025	− 546	1.025	601	659	20.84
	0.0050	− 531	0.543	681	714	58.06
	0.0075	− 532	0.398	721	764	69.26
	0.0100	− 520	0.1782	829	904	86.23
Quenched at 900 °C	0.0000	− 524	1.446	728	824	–
	0.0025	− 544	0.628	563	625	38.47
	0.0050	− 541	0.512	642	648	64.85
	0.0075	− 528	0.242	678	739	77.07
	0.0100	− 523	0.209	712	803	81.39

sodium and reduced amount of oxygen. These observations confirm the inhibitor being adsorbed on the metal surface.

3.8 X-Ray Diffraction (XRD) Analysis

XRD is one of the most used techniques for materials characterization. This is an excellent tool for the identification of the atomic scale periodicity or crystallinity of a material. As a result, this method works well for determining the species that makeup corrosion products that result from a reaction with an aqueous solution (Ref 49). This prompts us to methodically carry out XRD analysis on the surface of EN 8 steel under various heat-treated conditions. Figure 16 and 17 shows the detail of XRD plots corresponding to the phases on the EN 8 steel surface exposed to aqueous H_2SO_4 solution in the presence and in the absence of SBDS. Regardless of the heat treatment, it is observed that the peak ferrite phase (110) dominates all samples. It is extremely challenging to use the XRD to distinguish between the martensite and ferrite phases due to their overlap (Ref 50, 51). A further peak (200) can be seen for the metal sample, which also indicates the ferrite phase of EN 8 steel. The XRD plots obtained from the EN 8 surface in the presence of SBDS are essentially similar to that obtained for blank (Fig. 16). The pattern dint had any additional peaks indicating no complex formation on the EN 8 surface. This indicates that SBDS may be adsorbed on the EN 8 surface via physisorption rather than chemisorption to form a protective barrier. This conclusion is also supported by the values of $\Delta G°_{ads}$ and $\Delta H°_{ads}$ that are derived from the Langmuir adsorption isotherm.

4. Conclusions

In this study, weight loss and electrochemical approaches were used to study the inhibition of SBDS on the corrosion of heat-treated dual-phase EN 8 steel in 0.5 M sulfuric acid solution. Based on the results obtained, we can conclude the following points:

- In a solution of 0.5 M H_2SO_4, the SBDS serves as an inhibitor to prevent corrosion of heat-treated EN 8 steel.
- In the weight-loss study, The IE of SBDS increases with the increase in concentration and decreases with temperature, due to the physical adsorption of SBDS onto the surface of the heat-treated EN 8 steel and obeyed Langmuir adsorption isotherm.
- The energy and enthalpy of activation demonstrated that the corrosion process was protected by a barrier.
- The negative value of entropy of the activation indicates

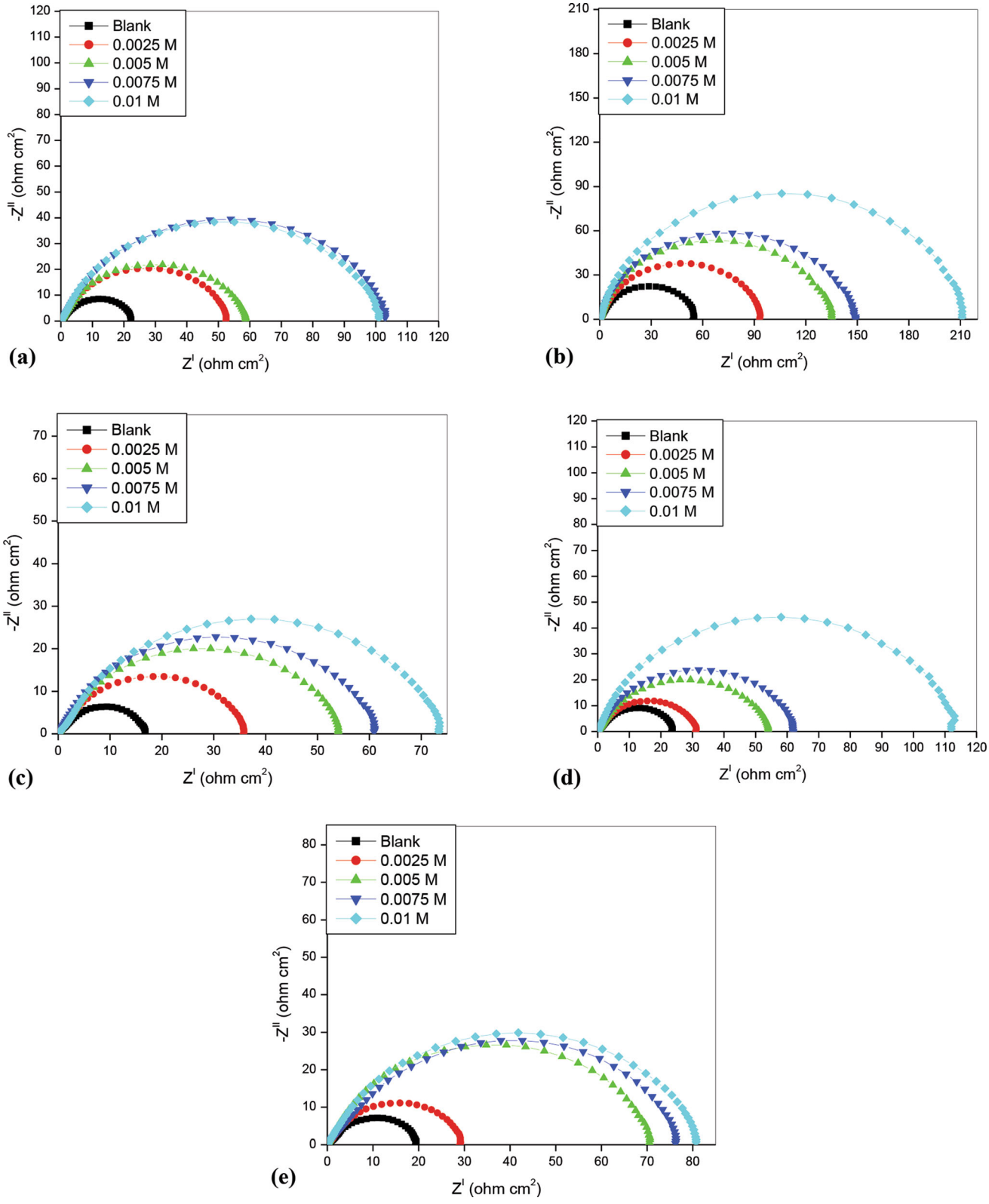

Fig. 11 Nyquist plots in 0.5 M H_2SO_4 containing different concentrations of SBDS at 303 K for the corrosion of (a) Normalized (b) Quenched at 700 °C (c) Quenched at 750 °C (d) Quenched at 790 °C (e) Quenched at 900 °C heat-treated phase of EN8 steel

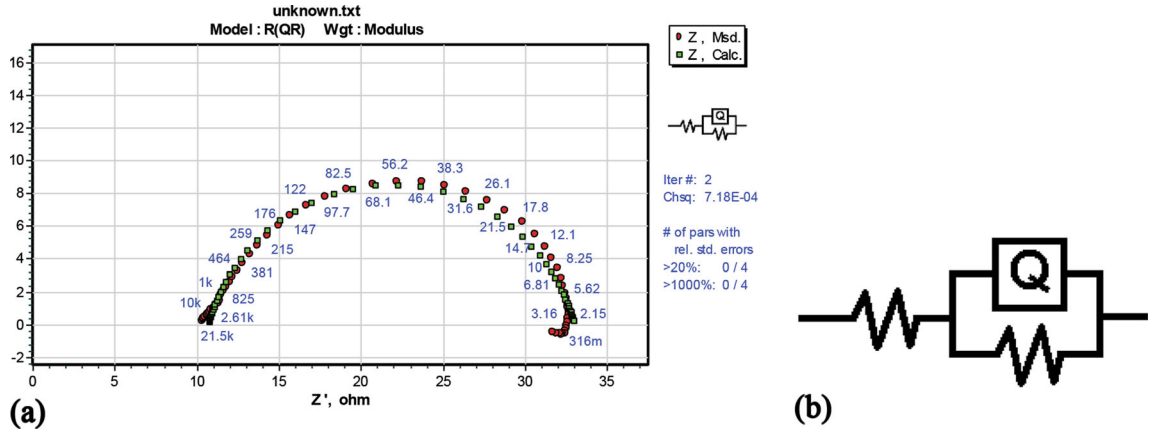

Fig. 12 (a) Representative ZSimpWin software fitting (b) Equivalent circuit used

Table 4 Results of EIS measurements for the inhibition of heat-treated EN8 steel in 0.5 M H_2SO_4 containing SBDS at 303 K

Type of heat treatment	[Surfactant], M	R_s, Ω cm^2	*CPE*, × 10^{-3}	*n*	χ^2, × 10^{-4}	R_{ct}, Ω cm^2	R_p, Ω cm^2	C_{dl}, μ F cm^{-2}	*IE*, %
Normalized	0.0000	10.5	0.507	0.79	6.805	19.65	33.15	7.254	–
	0.0025	9.91	0.133	0.836	6.568	52.92	62.83	1.23	47.24
	0.0050	11.59	0.127	0.819	3.835	59.27	70.86	1.016	53.22
	0.0075	9.83	0.144	0.817	5.328	102.6	112.43	0.358	70.51
	0.0100	10.53	0.134	0.823	3.044	104.7	115.23	0.356	71.23
Quenched at 700 °C	0.0000	8.732	0.09	0.859	11.54	55.28	64.01	10.86	–
	0.0025	8.812	0.071	0.858	4.911	94.47	103.28	0.402	38.02
	0.0050	11.68	0.063	0.864	2.009	136.3	147.98	0.2	56.74
	0.0075	11.5	0.055	0.868	1.578	148.7	160.2	0.17	60.04
	0.0100	14.6	0.054	0.873	1.519	312.9	327.5	0.081	80.45
Quenched at 750 °C	0.0000	10.71	0.482	0.797	5.383	22.3	33.01	5.531	–
	0.0025	7.26	0.247	0.807	5.964	36.28	43.54	2.689	24.18
	0.0050	8.23	0.246	0.798	4.935	55.05	63.28	1.239	47.84
	0.0075	8.93	0.191	0.816	2.285	61.63	70.56	0.976	53.22
	0.0100	11.84	0.197	0.801	5.089	74.57	86.41	0.677	61.80
Quenched at 790 °C	0.0000	7.232	0.32	0.808	11.74	23.91	31.14	5.569	–
	0.0025	7.505	0.231	0.814	8.068	31.41	38.91	3.39	19.97
	0.0050	7.939	0.167	0.835	3.366	58.74	66.67	1.056	53.29
	0.0075	7.445	0.142	0.831	4.484	62.75	70.19	0.941	55.63
	0.0100	7.534	0.115	0.846	3.365	114	121.53	0.297	74.38
Quenched at 900 °C	0.0000	9.68	0.507	0.79	6.805	17.04	26.72	9.112	–
	0.0025	10.21	0.201	0.834	8.594	29.01	39.22	3.536	31.87
	0.0050	9.767	0.117	0.824	3.472	71.23	80.99	0.728	67.00
	0.0075	9.405	0.246	0.755	1.328	79.25	88.65	0.634	69.85
	0.0100	10.57	0.172	0.801	3.178	82.18	92.75	0.568	71.19

that molecules are interacting with one another through association.

- The proximity of the free energy of adsorption values to 20 kJ mol^{-1} suggested that SBDS adsorbs spontaneously on the metal surface.
- The exothermic process was represented by the enthalpy of adsorption, and the arrangement of the molecules on the metal's surface was represented by the entropy of adsorption.
- The optimum inhibition efficiency of 85.36% was observed for EN 8 steel quenched at 790 °C and the least of 69.57% was observed for metal quenched at 700 °C by the PDP technique.
- Additionally, PDP tests showed that SBDS acts as a mixed inhibitor by reducing both cathodic and anodic processes.
- Studies using SEM, EDS, and XRD have demonstrated that the surface inhibitor film slows the rate of corrosion

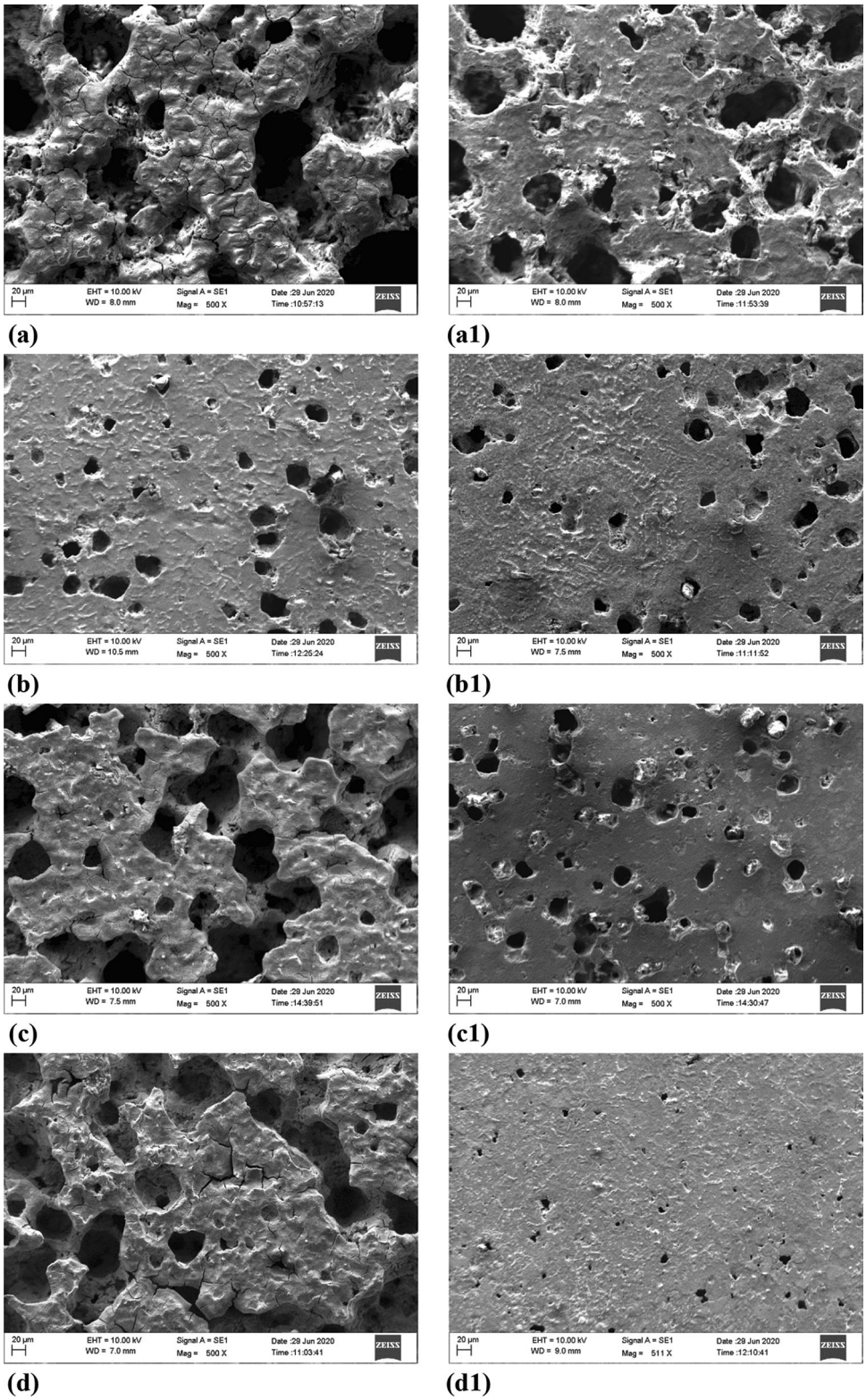

Fig. 13 SEM images in 0.5 M H_2SO_4 containing different concentrations of surfactant at 35 °C for the corrosion of EN 8 steel (a) Normalized (b) Quenched at 700 °C (c) Quenched at 750 °C (d) Quenched at 790 °C (e) Quenched at 900 °C

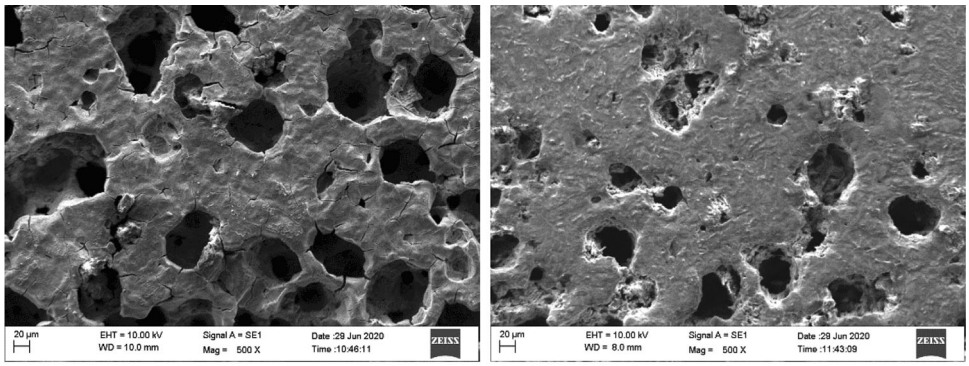

Fig. 13 continued

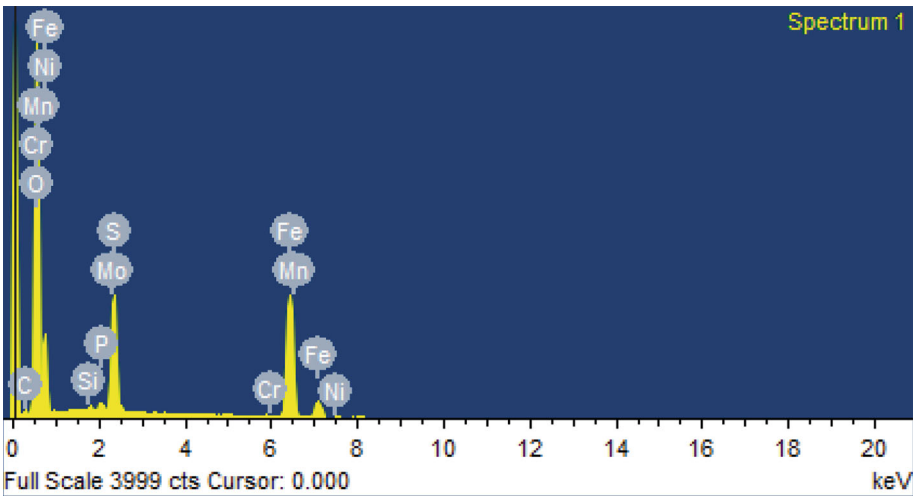

Fig. 14 EDS profile of EN 8 steel quenched at 790 °C in 0.5 M H_2SO_4—The wt.% of each elements are: C 2.45%, O 38.58%, Si 0.23%, P 0.56%, S 7.43%, Cr 0.02%, Mn 0.39%, Fe 48.28%, Ni 0.67%, Mo 1.39%

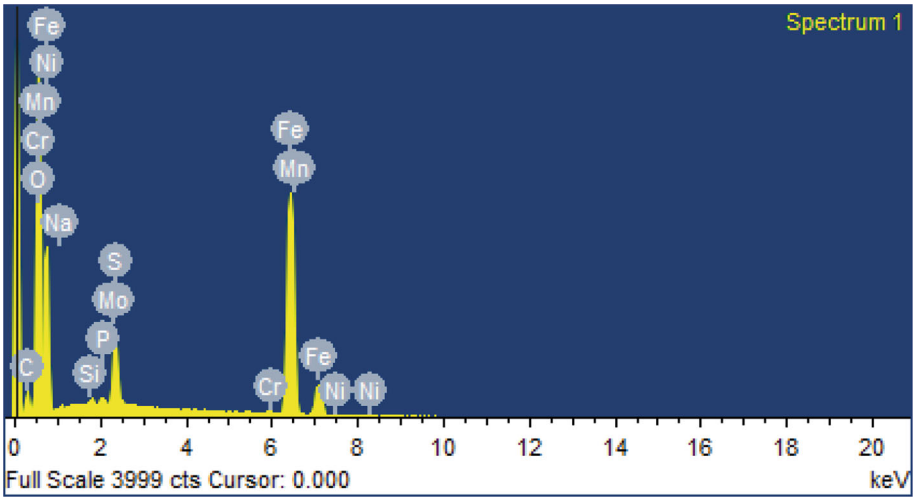

Fig. 15 EDS profile of EN 8 steel quenched at 790 °C in 0.5 M H_2SO_4 + 0.01 M SBDS—The wt.% of each elements are: C 5.02%, O 26.89%, Si 0.24%, P 0.24%, S 2.86%, Cr 0.14%, Mn 0.29%, Fe 63.12%, Ni 0.03%, Mo 1.08%

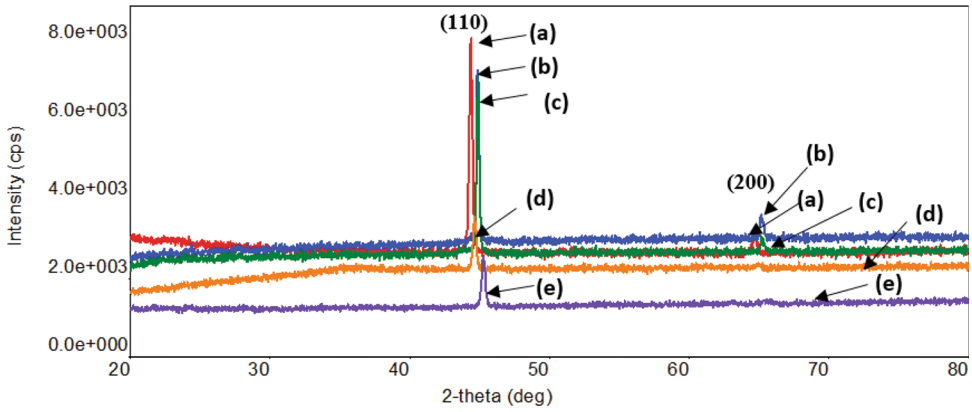

Fig. 16 XRD profile of a corroded sample of heat-treated materials in 0.5 M H_2SO_4, RED—quenched at 700 °C; BLUE—quenched at 750 °C; GREEN—quenched at 790 °C; ORANGE—Normalized; VIOLET—quenched at 900 °C

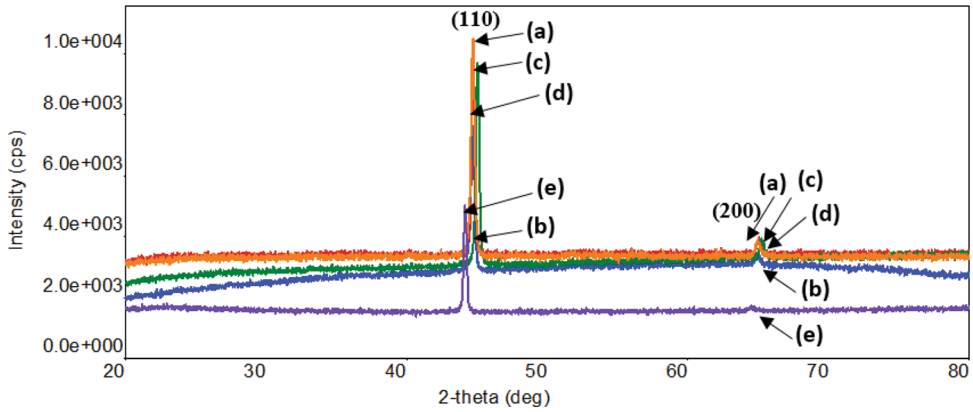

Fig. 17 XRD profile of a corroded sample of heat-treated materials in 0.5 M H_2SO_4 with SBDS, RED—Normalized; BLUE—quenched at 900 °C; GREEN—quenched at 700 °C; YELLOW—quenched at 750 °C; VIOLET—quenched at 790 °C

in heat-treated EN 8 steel when placed in a 0.5 M H2SO4 solution.

Acknowledgments

The authors acknowledge the facilities extended by the Department of Mechanical & Manufacturing Engineering, Department of Chemistry, and Central Instrumentation facility of Manipal Institute of Technology, Manipal Acadamy of Higher Education, Manipal.

Funding

Open access funding provided by Manipal Academy of Higher Education, Manipal. The authors received no direct funding for this research article.

Data availability

Inquiries about data availability should be directed to the corresponding author.

Conflict of interest

On behalf of all authors, the corresponding author claims no conflict of interest.

References

1. H.S. Abdo, A.H. Seikh, B.B. Mandal, J.A. Mohammed, S.A. Ragab, and M.S. Abdo, Microstructural Characterization and Corrosion-Resistance Behavior of Dual-Phase Steels Compared to Conventional Rebar, *Crystals*, 2020, **10**(11), p 1068.
2. L. Sharma and R. Chhibber, Effect of Heat Treatment on Mechanical Properties and Corrosion Behaviour of API X70 Linepipe Steel in Different Environments, *Trans. Indian Inst. Met.*, 2019, **72**(1), p 93–110.
3. N.O. Obi-Egbedi, I.B. Obot, and S.A. Umoren, *Spondias mombin* L. as a Green Corrosion Inhibitor for Aluminium in Sulphuric Acid: Correlation between Inhibitive Effect and Electronic Properties of Extracts Major Constituents Using Density Functional Theory, *Arab. J. Chem.*, 2012, **5**(3), p 361–373.
4. A. Saxena, V. Sharma, K.K. Thakur, and N. Bhardwaj, Electrochemical Studies and the Surface Examination of Low Carbon Steel by Applying the Extract of Citrus sinensis, *J. Bio- Tribo-Corrosion*, 2020, **6**(2), p 41.
5. M.C. Bignozzi et al., Effect of Heat Treatment Conditions on Retained Austenite and Corrosion Resistance of the X190CrVMo20-4-1 Stainless Steel, *Met. Mater. Int.*, 2020, **26**(9), p 1318–1328.
6. S.K. Basantia, A. Bhattacharya, N. Khutia, and D. Das, Plastic Behavior of Ferrite-Pearlite, Ferrite-Bainite and Ferrite-Martensite Steels: Experiments and Micromechanical Modelling, *Met. Mater. Int.*, 2021, **27**, p 1025.
7. D. Prabhu, J. Jomy, and P.R. Prabhu, Influence of Different Heat Treatment Temperatures on the Microstructure and Corrosion Behaviour of Dual-Phase EN8 Steel in 0.5 M Sulphuric Acid Solution, *J. Bio- Tribo-Corrosion*, 2022, **8**(4), p 88.
8. K. Mizuno, A. Nylund, and I. Olefjord, Surface Reactions during Pickling of an Aluminium-Magnesium-Silicon Alloy in Phosphoric Acid, *Corros. Sci.*, 2001, **43**(2), p 381–396.
9. W. Handoko, F. Pahlevani, and V. Sahajwalla, Effect of Austenitisation Temperature on Corrosion Resistance Properties of Dual-Phase High-Carbon Steel, *J. Mater. Sci.*, 2019, **54**(21), p 13775–13786.
10. Z. Xiong, A.G. Kostryzhev, Y. Zhao, and E.V. Pereloma, Microstructure Evolution during the Production of Dual Phase and Transformation Induced Plasticity Steels Using Modified Strip Casting Simulated in the Laboratory, *Metals*, 2019, **9**(4), p 449.
11. O. Keleştemur and S. Yıldız, Effect of Various Dual-Phase Heat Treatments on the Corrosion Behavior of Reinforcing Steel Used in the Reinforced Concrete Structures, *Constr. Build. Mater.*, 2009, **23**(1), p 78–84.
12. O. Abedini, M. Behroozi, P. Marashi, E. Ranjbarnodeh, and M. Pouranvari, "Intercritical Heat Treatment Temperature Dependence of Mechanical Properties and Corrosion Resistance of Dual Phase Steel," *Mater. Res.*, 2019, **22**
13. M. Manssouri, M. Znini, Z. Lakbaibi, A. Ansari, and Y. El Ouadi, Experimental and Computational Studies of Perillaldehyde Isolated from Ammodaucus leucotrichus Essential Oil as a Green Corrosion Inhibitor for Mild Steel in 1.0 M HCl, *Chem. Pap.*, 2021, **75**(3), p 1103–1114.
14. F. Branzoi, A. Băran, A. Ludmila, and E. Alexandrescu, The Inhibition Action of Some Organic Polymers on the Corrosion Carbon Steel in Acidic Media, *Chem. Pap.*, 2020, **74**(12), p 4315–4335.
15. N.T. Hoai et al., An Improved Corrosion Resistance of Steel in Hydrochloric Acid Solution Using Hibiscus sabdariffa Leaf Extract, *Chem. Pap.*, 2019, **73**(4), p 909–925.
16. M. Pais and P. Rao, Electrochemical, Spectroscopic and Theoretical Studies for Acid Corrosion of Zinc Using Glycogen, *Chem. Pap.*, 2021, **75**(4), p 1387–1399.
17. P.R. Prabhu, P. Hiremath, D. Prabhu, M.C. Gowrishankar, and B.M. Gurumurthy, Chemical, Electrochemical, Thermodynamic and Adsorption Study of EN8 Dual-Phase Steel with Ferrite-Martensite Structure in 0.5 M H_2SO_4 Using Pectin as Inhibitor, *Chem. Pap.*, 2021, **75**(11), p 6083–6099.
18. Y. Zhu, M.L. Free, R. Woollam, and W. Durnie, A Review of Surfactants as Corrosion Inhibitors and Associated Modeling, *Prog. Mater. Sci.*, 2017, **90**, p 159–223.
19. K. Shalabi, A.M. Helmy, A.H. El-Askalany, and M.M. Shahba, New Pyridinium Bromide Mono-Cationic Surfactant as Corrosion Inhibitor for Carbon Steel during Chemical Cleaning: Experimental and Theoretical Studies, *J. Mol. Liq.*, 2019, **293**, p 111480.
20. M.H. Sliem et al., AEO7 Surfactant as an Eco-Friendly Corrosion Inhibitor for Carbon Steel in HCl solution, *Sci. Rep.*, 2019, **9**(1), p 2319.
21. P.R. Prabhu, D. Prabhu, A. Chaturvedi, and P. Kishore Dodhia, Corrosion Inhibition of Ferrite Bainite AISI1040 Steel in H_2SO_4 Using Biopolymer, *Cogent Eng.*, 2021, **8**(1), p 1950304.
22. D. Prabhu, P.R. Prabhu, and P. Rao, Thermodynamics, Adsorption, and Response Surface Methodology Investigation of the Corrosion Inhibition of Aluminum by Terminalia Chebula Ritz. Extract in H3PO4, *Chem. Pap.*, 2021, **75**(2), p 653–667.
23. S.K. Hait, P.R. Majhi, A. Blume, and S.P. Moulik, A Critical Assessment of Micellization of Sodium Dodecyl Benzene Sulfonate (SDBS) and Its Interaction with Poly(Vinyl Pyrrolidone) and Hydrophobically Modified Polymers, JR 400 and LM 200, *J. Phys. Chem. B*, 2003, **107**(15), p 3650–3658.
24. A. G1-03(2017)e1, "Standard Practice for Preparing, Cleaning, and Evaluating Corrosion Test Specimens," *ASTM Int. West Conshohocken, PA*, 2017
25. D. Prabhu, S. Sharma, P.R. Prabhu, J. Jomy, and R.V. Sadanand, Analysis of the Inhibiting Action of Pectin on Corrosion of AISI1040 Dual-Phase Steel with Ferrite-Martensite and Ferrite-Bainite Structure: A Comparison in 0.5 M Sulphuric Acid, *J. Iran. Chem. Soc.*, 2021, **19**, p 1109–1128.
26. P.R. Prabhu, D. Prabhu, S. Sharma, and S.M. Kulkarni, Surface Properties and Corrosion Behavior of Turn-Assisted Deep-Cold-Rolled AISI 4140 Steel, *J. Mater. Eng. Perform.*, 2020, **29**(9), p 5871–5885.
27. P.R. Prabhu, D. Prabhu, and P. Rao, Analysis of Garcinia Indica Choisy Extract as Eco-Friendly Corrosion Inhibitor for Aluminum in Phosphoric Acid Using the Design of Experiment, *J. Mater. Res. Technol.*, 2020, **9**(3), p 3622–3631.
28. K. Wijeratne, "Conducting Polymer Electrodes for Thermogalvanic Cells," 2018
29. P. Deepa and R. Padmalatha, Corrosion Behaviour of 6063 Aluminium Alloy in Acidic and in Alkaline Media, *Arab. J. Chem.*, 2017, **10**, p S2234–S2244.
30. D. Prabhu and P. Rao, *Coriandrum sativum* L.—A Novel Green Inhibitor for the Corrosion Inhibition of Aluminium in 1.0 M Phosphoric Acid Solution, *J. Environ. Chem. Eng.*, 2013, **1**(4), p 676–683.
31. E. Fereiduni and S.S. Ghasemi Banadkouki, Improvement of Mechanical Properties in a Dual-Phase Ferrite–Martensite AISI4140 Steel under Tough-Strong Ferrite Formation, *Mater. Des.*, 2014, **56**, p 232–240.
32. T. Olugbade and J. Lu, Enhanced Corrosion Properties of Nanostructured 316 Stainless Steel in 0.6 M NaCl Solution, *J. Bio- Tribo-Corrosion*, 2019, **5**(2), p 38.
33. Y. Kharbach et al., Anticorrosion Performance of Three Newly Synthesized Isatin Derivatives on Carbon Steel in Hydrochloric Acid Pickling Environment: Electrochemical, Surface and Theoretical Studies, *J. Mol. Liq.*, 2017, **246**, p 302–316.
34. M. Abdallah, Ethoxylated Fatty Alcohols as Corrosion Inhibitors for Dissolution of Zinc in Hydrochloric Acid, *Corros. Sci.*, 2003, **45**(12), p 2705–2716.
35. E.E. Oguzie, Corrosion Inhibition of Aluminium in Acidic And Alkaline Media by Sansevieria Trifasciata Extract, *Corros. Sci.*, 2007, **49**(3), p 1527–1539.
36. J. Wang and X. Guo, Adsorption Isotherm Models: Classification, Physical Meaning, Application and Solving Method, *Chemosphere*, 2020, **258**, p 127279.
37. I.M. Mejeha et al., Experimental and Theoretical Assessment of the Inhibiting Action of Aspilia Africana Extract on Corrosion Aluminium Alloy AA3003 in Hydrochloric Acid, *J. Mater. Sci.*, 2012, **47**(6), p 2559–2572.
38. G.T. Galo, A. de Morandim-Giannetti, F. Cotting, I.V. Aoki, and I.P. Aquino, Evaluation of Purple Onion (*Allium cepa* L.) Extract as a

Natural Corrosion Inhibitor for Carbon Steel in Acidic Media, *Met. Mater. Int.*, 2020, **27**, p 3238–3249.
39. A.S. Fouda, A.A. Al-Sarawy, F.S. Ahmed, and H.M. El-Abbasy, Corrosion Inhibition of Aluminum 6063 using Some Pharmaceutical Compounds, *Corros. Sci.*, 2009, **51**(3), p 485–492.
40. L. Tang, G. Mu, and G. Liu, The Effect of Neutral Red on the Corrosion Inhibition of Cold Rolled Steel in 1.0 M Hydrochloric Acid, *Corros. Sci.*, 2003, **45**(10), p 2251–2262.
41. X. Li, S. Deng and H. Fu, Allyl Thiourea as a Corrosion Inhibitor for Cold Rolled Steel in H3PO4 Solution, *Corros. Sci.*, 2012, **55**, p 280–288.
42. C. C. Nathan, *Corrosion Inhibitors*. National Association of Corrosion Engineers, 1973
43. C.M. Brett, The Application of Electrochemical Impedance Techniques to Aluminium Corrosion in Acidic Chloride Solution, *J. Appl. Electrochem.*, 1990, **20**(6), p 1000–1003.
44. H. Cesiulis, N. Tsyntsaru, A. Ramanavicius, and G. Ragoisha, The Study of Thin Films by Electrochemical Impedance Spectroscopy BT—Nanostructures and Thin Films for Multifunctional Applications: Technology, Properties and Devices, I. Tiginyanu, P. Topala, and V. Ursaki, Eds. Cham: Springer International Publishing, 2016, pp. 3–42
45. A. Rodríguez-Torres, O. Olivares-Xometl, M.G. Valladares-Cisneros, and J.G. González-Rodríguez, Effect of Green Corrosion Inhibition by Prunus Persica on AISI 1018 Carbon Steel in 0.5 M H_2SO_4, *Int. J. Electrochem. Sci.*, 2018, **13**, p 3023–3049.
46. P.K. Katiyar, S. Misra, and K. Mondal, Effect of Different Cooling Rates on the Corrosion Behavior of High-Carbon Pearlitic Steel, *J. Mater. Eng. Perform.*, 2018, **27**(4), p 1753–1762.
47. S. Kumar, A. Kumar, Vinaya, R. Madhusudhan, R. Sah, and S. Manjini, Mechanical and Electrochemical Behavior of Dual-Phase Steels Having Varying Ferrite–Martensite Volume Fractions, *J. Mater. Eng. Perform.*, 2019, **28** (6), p 3600–3613
48. W.R. Osório, L.C. Peixoto, L.R. Garcia, and A. Garcia, Electrochemical Corrosion Response of a Low Carbon Heat Treated Steel in a NaCl Solution, *Mater. Corros.*, 2009, **60**(10), p 804–812.
49. Y. Abboud et al., Corrosion Inhibition of Carbon Steel in Hydrochloric Acid Solution Using Pomegranate Leave Extracts, *Corros. Eng. Sci. Technol.*, 2016, **51**(8), p 557–565.
50. Z. Li, F. Wei, P. La, and J. Sheng, Enhancing Strength of Nanolaminate 1045 Steel Prepared by Aluminothermic Reaction through Multiple Warm Rolling, *Steel Res. Int.*, 2018, **89**(2), p 1700304.
51. A. García-Junceda, C. Díaz-Rivera, V. Gómez-Torralba, M. Rincón, M. Campos, and J.M. Torralba, Analysis of the Interface and Mechanical Properties of Field-Assisted Sintered Duplex Stainless Steels, *Mater. Sci. Eng. A*, 2019, **740–741**, p 410–419.